Front. Earth Sci. 2023, 17(1): 71−86
https://doi.org/10.1007/s11707-022-0992-3

RESEARCH ARTICLE

Factors influencing methane diffusion behaviors in micro-nano coal pores: a comprehensive study

Xianglong FANG[1,2], Dameng LIU[1,2], Yingfang ZHOU[3], Xiaobo LIU (✉)[4], Yidong CAI (✉)[1,2]

1 School of Energy Resources, China University of Geosciences, Beijing 100083, China
2 Coal Reservoir Laboratory of National Engineering Research Center of CBM Development & Utilization, China University of Geosciences, Beijing 100083, China
3 School of Engineering, Fraser Noble Building, King's College, University of Aberdeen, AB24 3UE Aberdeen, UK
4 Postdoctoral Workstation of Applied Technology Research Institute, Northeast Petroleum University, Daqing 163318, China

Abstract Gas diffusion in the coal matrix plays a significant role in forecasting the production performance of coalbed methane (CBM) wells. To better understand methane diffusion behavior, a systematic study was performed on various rank coals with vitrinite reflectance ($R_{o,m}$) ranging from 0.46% to 2.79%. Multiple experiments, including coal petrographic analysis, field emission scanning electron microscopy (FESEM), low-temperature N_2 adsorption/desorption, and mercury intrusion porosimetry (MIP), were conducted to quantitatively characterize the multiscale micro-nano pore system in different rank coals, which showed that the pore structure of coals exhibited a multimodal pore size and volume distribution. Isothermal adsorption-diffusion experiments using the volumetric method were also performed to understand the methane diffusion characteristics in the micro-nano pores of the coal reservoir. The applicability of the multiporous diffusion model is verified, and methane diffusion in the multi-scale pores of coal reservoirs exhibits the characteristics of early fast diffusion, transitional diffusion in the medium term, and slow diffusion in the later period. In addition, the factors affecting methane diffusion in coals were systematically analyzed, and gray relational analysis (GRA) was employed to analyze and identify the importance of these factors on methane diffusion. The results show the impact ranking of factors, in order from the most important to the least: particle size > moisture > surface area > pore volume > pressure > coal rank > temperature in all of three diffusion stages. These findings are helpful for forecasting production performance and enhancing the production efficiency of CBM.

Received December 24, 2021; accepted March 31, 2022

E-mail: liuxiaobokm@126.com (Xiaobo LIU)
yidong.cai@cugb.edu.cn (Yidong CAI)

Keywords coalbed methane reservoir, micro-characteristic, diffusion coefficient, grey relational analysis

1 Introduction

Coalbed methane (CBM) is an abundant and low-cost fuel with significant long-term potential for discovery and development. The production and recovery rates of CBM are mainly controlled by gas diffusion in the coal matrix and permeability within the pore-fracture system (Busch et al., 2004; Lu et al., 2020; Jia et al., 2021). Diffusion theory tells us how methane molecules move from one place to another (from one pore to the next until the methane molecule reaches a cleat 'superhighway') (Moore, 2012). This should be addressed in CBM exploitation planning and economic reserve estimation. Based on this, there is a growing interest in understanding coal micro-nano pore characteristics, which affect the gas transport behavior and the mechanisms of adsorption-desorption and storage of methane in coal. A coal reservoir is characterized as a dual-porosity system (Warren and Root, 1963) that consists of cleats and a pore structure in the coal matrix. Based on their contribution to gas accumulation and migration, coal pores are divided into adsorption pores (including micropores and transition pores) and seepage pores (including mesopores and macropores) (Yao et al., 2008; Zhang et al., 2010). In this study, coal pores were divided into micropores (<10 nm), transition pores (10–100 nm), mesopores (100–1000 nm), and macropores (>1000 nm) (Zhang et al., 2010). Micro-structural characterization techniques for coal reservoirs can be systematically divided into two categories: 1) fluid injection methods, including CO_2/N_2 adsorption/desorption, mercury intrusion porosimetry (MIP), and nuclear

magnetic resonance (NMR) (Liu et al., 2018a; Zheng et al., 2018; Quan et al., 2020; Wang et al., 2020; Zhang et al., 2020; Bai et al., 2021), and 2) non-fluid injection methods, including scanning electron microscopy (SEM), transmission electron microscopy (TEM), atomic force microscopy (AFM), small-angle X-ray scattering (SAXS), small-angle neutron scattering (SANS), and X-ray computed tomography (CT) (Karacan and Okandan, 2001; Lu et al., 2020; Zhang et al., 2020; Zhao et al., 2020; Chen et al., 2021).

CBM transport in coal occurs in three stages: desorption (release of adsorbed methane), diffusion (controlled by the concentration gradient), and seepage (controlled by a pressure gradient) (Smith and Williams, 1984; Zhang et al., 2010). Several diffusion processes occur in coals, such as Fickian diffusion, Knudsen diffusion, and surface diffusion (Rigby, 2005; Pan et al., 2010; Zeng et al., 2019). In addition, a density model was proposed to describe the nonlinear gas diffusion behavior in a coal matrix, which exhibited a higher accuracy than the Fick model (Liu et al., 2018b). The main research methods on CBM diffusivity include experimental tests (Pan et al., 2010; Staib et al., 2013; Xu et al., 2015), numerical analysis (Fang et al., 2018; Liu et al., 2019a; Yang et al., 2019) and molecular simulation (Hu et al., 2010; Si et al., 2021). In CBM diffusion studies, some scholars have demonstrated a negligible impact of sorption time on gas production from coalbeds (Bybee, 2004; Salmachi et al., 2014), but gas diffusivity in the coal matrix significantly affects the gas production rate (Pan et al., 2010). Gas diffusion may play an important role in the later stages of the life of a CBM reservoir. It may explain the increased production rates typically observed in the basin during the later part of the reservoir's life (Pillalamarry et al., 2011). Some researchers have suggested that using the diffusion coefficient as a direct input parameter would be more reasonable than using the sorption time (Pillalamarry et al., 2011). Owing to the complexity and heterogeneity of the coal pore structure, scholars have proposed the unipore diffusion model (Crank, 1956), bidisperse diffusion model (Ruckenstein et al., 1971; Smith and Williams, 1984; Clarkson and Bustin, 1999) and multiporous diffusion models (Li et al., 2016). The bidisperse diffusion model can be used to describe the methane diffusion of bituminous coal and anthracite with a relatively complex pore structure, whereas the unipore diffusion model is only applicable to bright coal with a relatively uniform pore structure (Clarkson and Bustin, 1999).

This is a crucial research topic regarding the factors affecting diffusion. According to previous studies, in the bidisperse model, CH_4 diffusivity would decrease first and then increase with coal rank, which showed an asymmetric "U" shape (Meng and Li, 2016). Thereafter, it would decrease gradually with the increase of moisture content (Meng and Li, 2016; Pan et al., 2010; Guo et al., 2018). In a porous diffusion model, the diffusion coefficient of macropores and micropores in low-rank coal decreases with increased pressure, whereas that of mesopores is positively correlated with pressure (Li et al., 2016). Coals with a high macroporosity content would have good gas flow capability, and the times for sorption equilibrium would increase with increasing grain size (Busch et al., 2004). Some researchers have suggested that gas diffusivities increase with pressure and temperature (Charrière et al., 2010; Cai et al., 2014), whereas Pillalamarry et al. (2011) found a negative correlation between the diffusion coefficient and pressure for pressures below 3.5 MPa. In addition, they insisted that the diffusion coefficient depends on adsorption or surface coverage, whereas Crosdale et al. (1998) supported the view that pore structure, rather than coal rank and maceral composition, is a critical factor in controlling gas diffusion.

As the factors influencing diffusion are controversial and the diffusion mechanism is not clear, a comprehensive investigation is required. In this study, multiple regular experiments were conducted to quantitatively characterize the multiscale micro-nano pore system in different rank coals. Isothermal adsorption-diffusion experiments using the volumetric method were also performed to investigate the characteristics and influencing factors of methane diffusion in the micro-nano pores of coal reservoirs based on different diffusion models. Finally, gray relational analysis was employed to integrate all information to determine the most crucial factor for CBM diffusion.

2 Theoretical background and experimental scheme

2.1 Diffusion model

Owing to the multiscale and complexity of the pore structure in coal reservoirs, scholars have proposed unipore, bidisperse, and multiporous diffusion models. Based on the assumptions of homogenous pore size in a coal reservoir, the relationship between the adsorption capacity and gas unipore diffusion coefficient can be obtained (Crank, 1956):

$$\frac{M_t}{M_\infty} = 1 - \frac{6}{\pi^2}\sum\nolimits_{n=1}^{\infty}\frac{1}{n^2}\exp\left(-D_e n^2\pi^2 t\right), \quad (1)$$

where M_t is the mass of gas desorbed at time t and M_∞ is the total mass of gas desorbed at equilibrium pressure; t is the time, s; D_e is defined as effective diffusivity, which can be expressed as $D_e = D/r_p^2$, D is the gas diffusion coefficient, m^2/s; r_p is the diffusion path length.

Smith and Williams (1984) and Clarkson and Bustin (1999) claimed that a homogeneous unimodal pore structure was only appropriate for modeling methane diffusivity in bright coals. They assumed that the coal reservoir had a bimodal pore size distribution. The

simplified bidisperse diffusion model includes a fast macropore diffusion stage and a slower micropore diffusion stage (Ruckenstein et al., 1971):

$$\frac{M_a}{M_{a\infty}} = 1 - \frac{6}{\pi^2}\sum_{n=1}^{\infty}\frac{1}{n^2}\exp\left(-D_{ae}n^2\pi^2 t\right), \quad (2)$$

$$\frac{M_i}{M_{i\infty}} = 1 - \frac{6}{\pi^2}\sum_{n=1}^{\infty}\frac{1}{n^2}\exp\left(-D_{ie}n^2\pi^2 t\right), \quad (3)$$

where M_a and M_i are the total mass of methane desorbed in the macropores and micropores, respectively, at time t. $M_{a\infty}$ and $M_{i\infty}$ are the total amount of methane desorbed in the macropores and micropores over infinite time, respectively, and D_{ae} and D_{ie} are the macropore and micropore effective diffusivities, respectively.

The studies on pore microstructure showed that the pore size distribution of coals is usually multi-peak (Cai et al., 2014). Based on the extremely complex structure of coal reservoirs, a multiporous diffusion model was proposed based on the bidisperse diffusion model (Li et al., 2016):

$$\frac{M_t}{M_\infty} = \sum_{\varphi=1}^{\infty}\frac{M_\varphi}{M_{\varphi\infty}} = \partial_1\frac{M_1}{M_{1\infty}} + \partial_2\frac{M_2}{M_{2\infty}} + \cdots + \left(1-\partial_1-\partial_2-\cdots-\partial_{\varphi-1}\right)\frac{M_\varphi}{M_{\varphi\infty}}, \quad (4)$$

where M_φ is the amount of methane desorbed at a certain pore scale at time t, $M_{\varphi\infty}$ is the total amount of methane desorbed at the same pore scale over infinite time, and ∂_φ is the ratio of desorption to the total desorption at a certain pore scale. In addition, $\partial_1 + \partial_2 + \ldots + \partial_\phi = 1$. In this study, φ was assigned a value of 3. Therefore, Eq. (4) can be expressed as

$$\frac{M_t}{M_\infty} = \frac{M_a + M_e + M_i}{M_{a\infty} + M_{e\infty} + M_{i\infty}} = \partial_a\frac{M_a}{M_{a\infty}} + \partial_e\frac{M_e}{M_{e\infty}} + \partial_i\frac{M_i}{M_{i\infty}}, \quad (5)$$

where M_e is the total amount of methane desorbed in the transition pores and mesopores (corresponding to the transition diffusion stage) at time t and $\partial_1 + \partial_2 + \partial_3 = 1$.

2.2 Coal samples and fundamental analysis

Considering the metamorphic grades and pore structure characteristics, 12 block coal samples were collected from the active mining areas of the eastern Junggar Basin, eastern Ordos Basin, and southern Qinshui Basin (Table 1), including four high-rank coals (SY 15#, XY 15#, DY 6#, GZ 15#), four medium-rank coals (YT 5#, HJG 5#, WJY 8#, DQ 4#), and four low-rank coals (LHJ 4#, FL 1#, HDG 6#, BD 2#). The maximum vitrinite reflectance ($R_{o,m}$) (immersion in oil) and maceral composition were acquired using a Laborlxe 12 POL microscope on polished surfaces following China National Standards GB/T 6948-2008 and GB/T 8899-2013. Proximate analysis was performed with an automatic proximate analyzer (5E-6600) following the Standards ISO 17246-2010 at the China University of Geosciences in Beijing (CUGB).

2.3 Microstructure characterization

Field emission scanning electron microscopy (FESEM)

Table 1 Sample basic information and structure analysis results of the selected coals

Sample No.	$R_{o,m}$/%	Maceral and mineral/(vol%)				Prox/(wt%, ad)				Low-temperature N_2 analysis			Mercury injection analysis					
		V	I	E	M	Mo	A	Vo	FC	S_{BET}/($m^2 \cdot g^{-1}$)	V_{BJH}/(10^{-3} $cm^3 \cdot g^{-1}$)	d_a/nm	Φ/%	Sa/%	E_{ex}/%	d_m/μm	V_n/($cm^3 \cdot g^{-1}$)	Curve types
LHJ 4#	0.46	78.80	5.40	12.1	3.8	6.46	6.09	39.11	48.34	0.559	2.282	18.03	6.17	89.75	43.02	0.431	0.104	I
FL 1#	0.65	78.00	12.20	7.00	2.8	5.78	15.8	16.2	62.20	0.116	0.467	15.38	4.31	76.38	34.6	0.250	0.088	II
HDG 6#	0.68	72.30	11.00	16.2	0.5	6.38	11.3	15.02	67.30	0.867	4.207	21.02	8.92	82.77	65.84	0.323	0.049	I
BD 2#	0.68	69.90	18.30	11.6	0.2	8.63	5.38	17.93	68.06	0.301	1.701	11.21	4.86	73.42	54.63	0.239	0.062	II
YT 5#	1.19	57.81	32.19	2.50	7.5	0.71	12	26.77	60.48	0.477	2.546	16.99	3.46	70.76	45.04	0.182	0.048	II
HJG 5#	1.34	60.68	25.02	0	14.3	0.74	10.3	27.94	61.05	0.367	1.232	13.43	2.98	58.56	61.65	0.314	0.037	II
WJY 8#	1.44	40.03	56.67	0	3.3	0.57	9.9	26.8	62.73	0.347	1.574	13.82	1.48	31.64	31.88	0.149	0.042	III
DQ 4#	1.68	59.69	34.61	0	5.7	0.63	11.1	21.3	66.97	0.378	1.279	10.60	3.1.3	89.04	30.65	0.329	0.031	I
SY 15#	2.05	76.97	16.33	0	6.7	0.71	11.6	48.97	38.75	0.487	2.339	16.52	1.58	30.72	15.51	0.244	0.023	III
XY 15#	2.54	77.98	15.52	0	6.5	1.43	11.1	12.46	75.05	0.246	0.867	15.22	1.79	31.77	23.77	0.125	0.016	III
DY 6#	2.56	49.51	7.99	0	42.5	0.62	38.1	15.94	45.36	0.375	1.595	15.20	4.66	90.37	33.52	0.355	0.015	I
GZ 15#	2.79	83.55	12.15	0	4.3	1.2	13.3	12.49	73.01	0.202	1.662	18.77	1.92	27.67	39.62	0.125	0.018	III

Notes: ad- as received basis; V- Vitrinite; I - Inertinite; E- Exinite; M- Mineral; Prox- Proximate analysis; Mo-Moistures; Vo-Volatiles; A-Ash; FC-Fixed Carbon; S_{BET} - BET surface area; V_{BJH} - BJH total pore volume; d_a- Average pore size; Φ - Porosity; Sa- Mercury saturation; E_{ex} - Extrusion efficiency; d_m - Average pore throat size; V_n - MIP total pore volume.

was used to observe the morphological characteristics of micropores in the coal reservoirs. Before FESEM imaging, one surface of the cube (~0.5 cm × 1 cm × 1 cm) was polished using dry emery paper and then polished again by argon ions (Desbois et al., 2011). Experiments were conducted at the Institute of Geology and Geophysics, Chinese Academy of Sciences, using the MERLIN high-resolution FESEM system produced by Zeiss.

Low-temperature N_2 gas adsorption/desorption experiments were used to characterize the pores with diameters between 1.7 to 300 nm. Before the experiment, the samples were ground and gridded to a particle size of 60–80 mesh (0.18–0.25 mm) and dried at 105°C for 24 h in a vacuum oven (Yao et al., 2008). The experiment was performed in the Coal Reservoir Petrophysical Laboratory of the China University of Geosciences (Beijing) with Micromeritics ASAP-2000.

MIP is a conventional technique for characterizing the pore structures of coal reservoirs. The tests were conducted using a PoreMasterGT60 at the Petrophysical Laboratory of China University of Geosciences (Beijing) following the Chinese Oil and Gas Industry Standard SY/T 5346-2005 (Zheng et al., 2018). Volume intrusion curves of mercury were obtained at pressures ranging from 0.0074 to 206 MPa, corresponding to diameters ranging between 100 and 0.0072 μm.

2.4 Volumetric diffusion experiment

The CH_4 diffusivity experiment was based on the volumetric method, which was performed using the TerraTek Isotherm Measurement System (IS–300) following the Chinese standard GB/T 19560-2004. The maximum pressure in the experimental process could reach 8.0 MPa with a maximum test temperature of 40°C, and the CH_4 desorption capacity was calculated using the volumetric method. The experimental and data processing procedures were the same as those presented in our previous studies (Yao et al., 2008; Fang et al., 2018). In addition, moisture-equilibrated samples were prepared, as described in detail by Pan et al. (2010).

2.5 Grey relational analysis

Grey relational analysis is an impacting measurement method in gray systems theory which analyzes uncertain relations between one main factor and all the other factors in a given system (Tosun, 2006). First, an original analysis sequence, which includes a reference sequence and a comparing sequence, should be determined. The reference sequence, consisting of methane diffusion coefficients, is denoted by $\{X_0^{(0)}(i)\},(i=1,2,\ldots,n)$. The comparing sequence which is denoted by $\{X_t^{(0)}(i)\}(t=1,2,\ldots,m),(\mathrm{i}=1,2,\ldots,n)$ is composed of several influencing factors of methane diffusion.

Data pre-processing is normally required since the range and unit in one data sequence may differ from the others. The original sequence can be simply normalized as follows:

$$\mathrm{X}_t^{(1)}(i)=\frac{\mathrm{X}_t^{(0)}(i)}{\mathrm{X}_t^{(0)}(1)}, \tag{6}$$

where t = 1, 2, …, m; i = 1, 2, …, n. The gray relation coefficient $\xi_t(i)$ for the ith performance characteristics in the ith experiment can be expressed as

$$\xi_t(i)=\frac{t_{\min}i_{\min}\left|X_0^{(1)}(i)-X_t^{(1)}(i)\right|+\rho t_{\max}i_{\max}\left|X_0^{(1)}(i)-X_t^{(1)}(i)\right|}{\left|X_0^{(1)}(i)-X_t^{(1)}(i)\right|+\rho t_{\max}i_{\max}\left|X_0^{(1)}(i)-X_t^{(1)}(i)\right|}, \tag{7}$$

where ρ is distinguishing coefficient: $\rho\in(0,1)$, and ρ = 0.5 is generally used. After that, the gray relational grade is defined by the average value of the gray relational coefficient:

$$r_{\mathrm{i}}=\frac{1}{n}\sum\nolimits_1^n\xi_t(\mathrm{i}), \tag{8}$$

where i = 1, 2, …, n.

3 Results

3.1 Coal basic information

Information regarding the 12 coal samples (including the maximum vitrinite reflectance, maceral and mineral contents, and proximate analysis) is shown in Table 1. The coals are subbituminous to anthracite, with mean maximum vitrinite reflectance in oil ($R_{\mathrm{o,m}}$) ranging from 0.46% to 2.79%. The volume contents for vitrinite, inertinite and exinite are in the range of 40.03%–83.55%, 5.4%–56.67% and 0%–16.2%, respectively. Exinite cannot be identified when $R_{\mathrm{o,m}}$ is over 1.19%. The mineral content in coal markedly varies from 0.2% to 42.5%, which is related to the sedimentary environment. Figure 1 shows the oil-immersed photographs of the six samples under reflected light using a polarizing microscope. The cell walls are broken and filled with a lot of clay (Cl), and pyrite particles (Py) are randomly distributed in semitelinite (Figs. 1(a), 1(b), and 1(c)). The collinite (C) is widely distributed in the sample DY 6#, and the microsomes (Mi) are densely banded in GZ 15# (Figs. 1(c) and 1(d)). The moisture content in low rank coal is obviously higher (5.78%–8.63%) than in medium-high rank coal (0.57%–2.01%). Volatile material content varies from 3.5% to 48.97%, and fixed carbon content ranges between 38.75% and 75.05%. The ash yield varies markedly, ranging from 5.38% to 38.08%, and its main composition is aluminosilicate which is controlled by the sedimentary environment of coal accumulation.

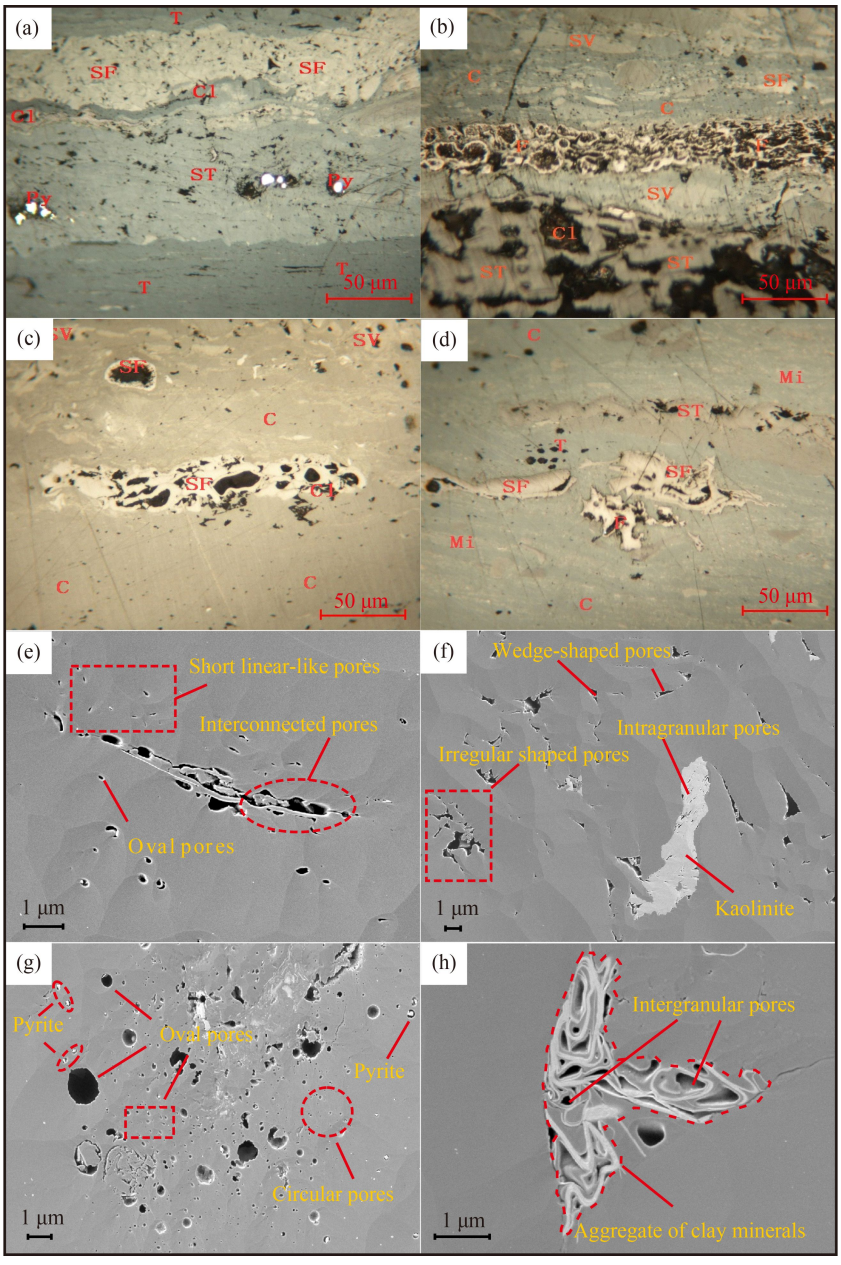

Fig. 1 Oil-immersed photographs of maceral and minerals and FESEM images of pore structure in different rank coals. (a) HJG 5#, $R_{o,m}$ = 1.34%, 200 × ; (b) DQ 4#, $R_{o,m}$ = 1.52%, 200 × ; (c) DY 6#, $R_{o,m}$ = 2.56%, 200 × ; (d) GZ 15#, $R_{o,m}$ = 2.79%, 200 × ; (e) YT 5#, $R_{o,m}$ = 1.19%, 10650 × ; (f) SY 15#, $R_{o,m}$ = 2.05%, 4140 × ; (g) XY 15#, $R_{o,m}$ = 2.54%, 6350 × ; (h) DY 6#, $R_{o,m}$ = 2.56%, 14940 × .

Notes: T: telinite; ST: semitelinite; C: collinite; SV: semivitrinite; F: fusinite; SF: semifusinite; Cl: clay; Py: pyrite; Mi: microsome.

3.2 Pore structure characteristics

The morphology of pore fractures from FESEM images is shown in Fig. 1, and the pores in the coals are divided into primary pores, metamorphic pores, and mineral-related pores (Zhang, 2001). For low-rank bituminous coals, gas pores were generated during the decomposition of organic matter in the initial stage of coal formation, whose initial shape was round; however, they were compressed into irregular shapes by formation pressure. As a result, irregularly shaped organic matter pores with small radii (<100 nm) were dispersed in the coal matrix, such as oval pores (accounting for approximately 20%), wedge-shaped and slit-like pores (accounting for approximately 50%), and short linear-like pores (accounting for approximately 20%) (Figs. 1(e), 1(f), and 1(g)). With the process of coalification, many metamorphic pores (accounting for approximately 70%) appeared with a cluster distribution in the organic matter in high-rank bituminous coal and anthracite, and their pore size increased to 100–1500 nm with better pore connectivity (Fig. 1(g)). In addition, a few pores were filled with

minerals that would affect pore connectivity and gas diffusions, such as metallic minerals (pyrite) and clay minerals (kaolinite and illite) (Figs. 1(f), 1(g), and 1(h)).

The BET pore surface area, BJH total pore volume, and pore size distribution obtained from low-temperature N_2 adsorption/desorption experiments are shown in Table 1. The surface areas ranged from 0.1156 to 0.8667 $m^2 \cdot g^{-1}$, and the averages of the surface areas showed the following trend: low-rank coal > medium-rank coal > high-rank coal (Fig. 2(a)). The average pore diameters of coal samples are between 11.21 and 21.02 nm, and the total pore volumes of coal are positively correlated with surface areas (Fig. 2(b)), which is consistent with the conclusion 8 of Zhao et al. (2016).

The parameters, such as porosity, total pore volume, mercury saturation, and mercury extrusion efficiency obtained by MIP, are shown in Table 1. The porosity of all the samples ranged from 1.48 to 8.92%, among which the porosity of low-rank coal was larger (4.31% to 8.92%) than that of medium-high rank coal (1.48%–4.66%). The mean diameter of the pores in the different ranks of coal ranged from 0.226 to 8.18 μm. The variations in mercury saturation and mercury extrusion efficiency were significant, with values ranging from 27.67%–90.37% and 15.51%–65.84%, respectively.

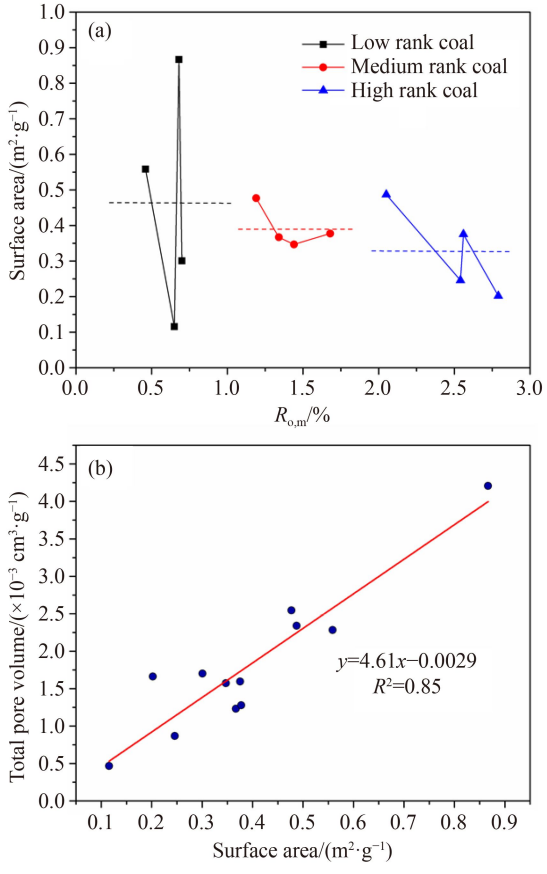

Fig. 2 (a) The relationship between pore surface area and coal rank; (b) The relationship between total pore volume and pore surface area.

According to previous studies, samples with a higher mercury withdrawal efficiency may have a more uniform pore structure and better connectivity, conducive to the diffusion and seepage of coalbed methane (Zhang et al., 2010).

Micropores and transition pores (<10^2 nm), mesopores (10^2–10^3 nm), and macropores (>10^3 nm) accounted for 19.57%–69.08%, 4.2%–55.65%, and 4.36%–70.64% of the total pore volume in the samples, respectively. Based on a summary of previous studies, mercury injection curves were divided into three categories in this study (Fig. 3), and the specific classification criteria were the same as those presented in our previous study (Fang et al., 2018). The mercury intrusion-extrusion curves and pore volume distributions of typical coal samples are listed in Table 1.

3.3 Methane diffusion characteristics in micro-nano pores

The CH_4 effective diffusion coefficients under the bidisperse and multiporous models were obtained through data fitting using Origin and MATLAB (see Supplementary material). Based on the bidisperse diffusion model, the effective diffusion coefficient of macropores is within the order of magnitude of approximately 10^{-5}–10^{-4} s^{-1}, whereas that of micropores is 10^{-6}–10^{-5} s^{-1}. In contrast, based on the multiporous model, the order of magnitude of the macropore diffusivity (M_{ae}) was between 10^{-4} and 10^{-3} s^{-1}, the transition pores and mesopore diffusivity (M_{ee}) ranges from 10^{-5} to 10^{-4} s^{-1}, and the micropore diffusivity (M_{ie}) ranges from 10^{-6} to 10^{-5} s^{-1}. The macropore diffusivities (M_{ae}) calculated by the bidisperse model are between the values of M_{ae} and M_{ee} calculated by the multiporous model, which is consistent with the results of Li et al. (2016).

Figure 4 shows the fit curves of the bidisperse and multiporous models for the different ranks of coals. The multiporous model shows an excellent fit to the diffusion data, whereas the fitting curve of the bidisperse model shows a partial deviation from the data points. The deviation between the fitting curve of the bidisperse model and the data was significant in DY 6# and GZ15. This difference indicates that the bidisperse model has some errors in characterizing CH_4 adsorption-diffusion behavior, whereas the multiporous model is more in line with the CBM adsorption-diffusion process by considering the transition diffusion stage. This conclusion is also reflected in the goodness of fit in Supplementary material.

By analyzing the diffusion coefficient based on the multiporous model, it was found that the average macropore effective diffusion coefficient (M_{ae}) for low-rank coals is 3.85 × 10^{-3} s^{-1}, and that of the transition diffusivity (M_{ee}) and micropore diffusivity (M_{ie}) are 1.17 × 10^{-4} s^{-1} and 1.48 × 10^{-5} s^{-1}, respectively. For medium-rank coals, the mean values of the macropore diffusivity were 1.01 × 10^{-3} s^{-1}, that of transition

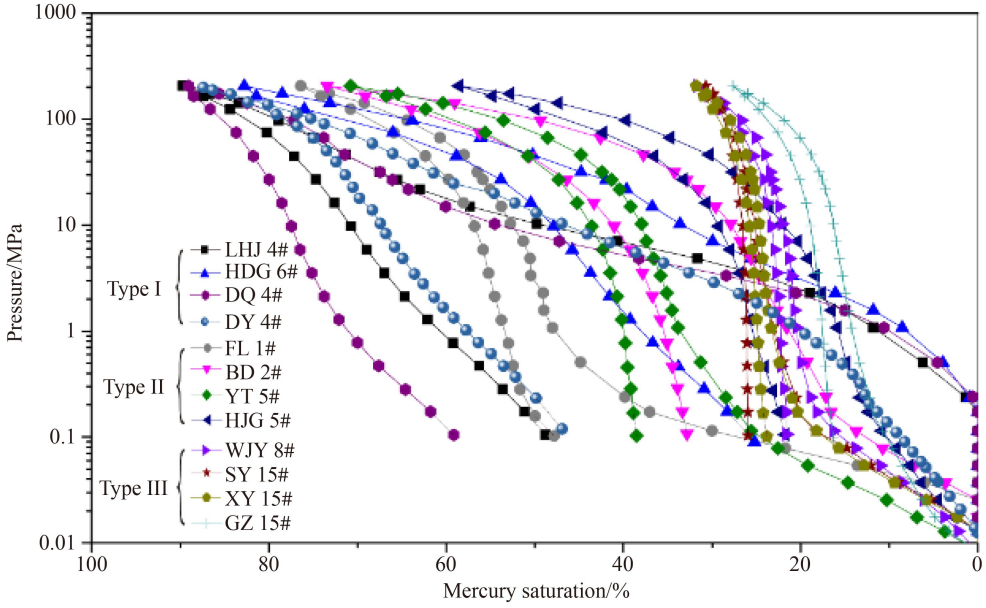

Fig. 3 The mercury intrusion-extrusion curves of different rank coals.

diffusivity, and micropore diffusivity were 4.79×10^{-5} s^{-1} and 5.94×10^{-6} s^{-1}, respectively. For high-rank coals, the average macropore diffusivity is 3.98×10^{-3} s^{-1}, and those of transition pores, mesopores, and micropore are 1.22×10^{-4} s^{-1} and 1.31×10^{-5} s^{-1}, respectively.

In addition, several groups of comparative experiments were also set in this study, and the multiporous diffusion coefficients were obtained, as shown in Supplementary material. FL 1# and GZ 15# were selected and ground into 0.18–0.25 mm (60–80 mesh), 1.7–3.35 mm (6–10 mesh) and 6.7–8 mm (2–3 mesh), respectively, for particle size contrast experiment. The order of magnitude of the macropore and micropore diffusivities of the three particle size samples was 10^{-3} s^{-1} and 10^{-4} s^{-1}, respectively. In the transition diffusion stage, the effective diffusion coefficients of the 60–80 mesh samples vary from 10^{-5} to 10^{-4} s^{-1}, whereas that of the 6–10 mesh and 2–3 mesh samples are 10^{-4} s^{-1}. LHJ 4# and GZ 15# were selected for drying and equilibrium moisture, respectively, and each group of samples was divided into three states: dry, semi-equilibrium, and equilibrium moisture. In the macropore diffusion stage, the order of magnitude of the diffusivity with dry and equilibrium samples was 10^{-3} s^{-1} and 10^{-4} s^{-1}, respectively, whereas the effective diffusion coefficients of the semi-equilibrium moisture samples vary from 10^{-4} to 10^{-3} s^{-1}. In the transition diffusion stage, the order of magnitude of the diffusivity with dry samples was 10^{-4} s^{-1}, whereas that of the semi-equilibrium and equilibrium samples was 10^{-5} s^{-1}. In the micropore diffusion stage, the diffusivity of dry samples is within the order of magnitude of 10^{-5} s^{-1}, and that of semi-equilibrium and equilibrium samples was 10^{-6} s^{-1}. To investigate the impact of temperature on methane diffusion, two groups of additional diffusion experiments at 40°C were performed using BD 2# and SY 15#, and the order of magnitude of the macropore diffusivity, transition diffusivity, and micropore diffusivity was 10^{-3} s^{-1}, 10^{-4} s^{-1}, and 10^{-5} s^{-1}, respectively.

4 Discussion

4.1 Factors affecting methane diffusion

Methane diffusion in coal reservoir is affected by coal rank, pore structure, particle size, moisture content, temperature, and pressure (Figs. 5(a)–5(f)). To analyze the mechanism of methane diffusion in coal, each influencing factor was studied separately using the control variable method.

4.1.1 Pore structure

The test range of pore diameter using N_2 adsorption/desorption method is 1.7–300 nm, and that of the MIP is 7–10^5 nm (Zhang et al., 2010). In the mercury intrusion porosimetry, matrix shrinkage occurs in coals when the pressure reaches 7.06 MPa (Cai et al., 2018), indicating that errors occur in the pore data with the corresponding pore diameter below 100 nm. To qualitatively analyze the relationship between the diffusion coefficient ratio (∂) and pore volume/surface area at various scales of coal reservoirs, a new group of integrated data was selected and spliced from the front segment of the N_2 adsorption/desorption experiment results (<100 nm) and the back segment of the MIP results (>100 nm). The integrated data were divided into three sections (<10, 10–1000 nm, >1000 nm), which correspond to the stages of micropore diffusion, transition diffusion, and macropore diffusion in the multiporous diffusion, respectively (Table 2).

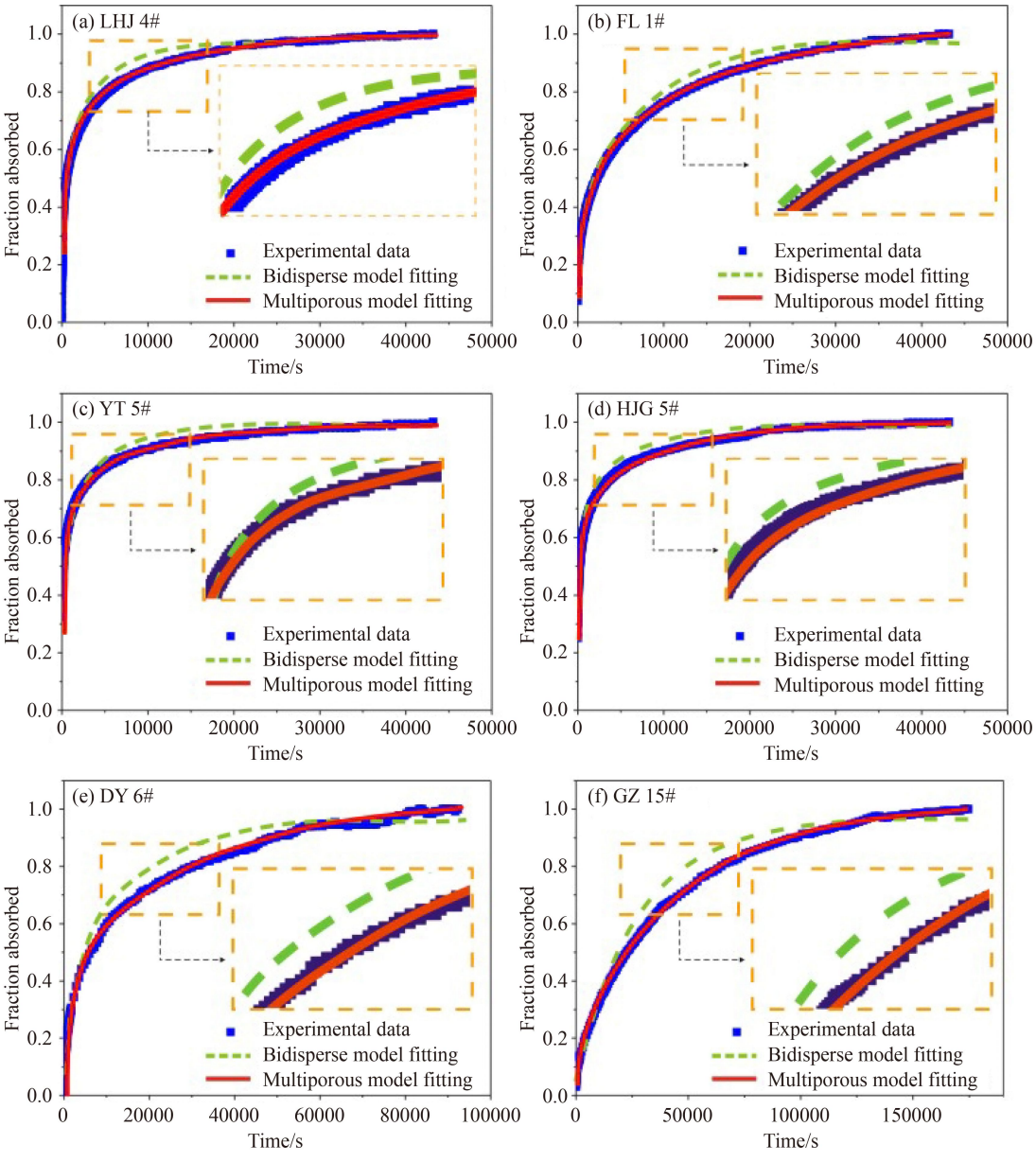

Fig. 4 Fitting curves of experimental data using bidisperse and multiporous diffusion model.

A composite graph of the diffusion coefficient ratio (∂) and pore volume/surface area fraction of different diffusion stages was plotted to reveal the relationship between methane diffusivity and pore structure (Fig. 6). The entire diffusion process can be divided into three parts: a fast macropore diffusion stage corresponding to macropores (>1000 nm), an intermediate rate transition diffusion stage corresponding to transition pores and mesopores (10–1000 nm), and a much slower micropore diffusion stage corresponding to micropores (<10 nm). It is apparent that the samples with relatively high pore volumes also have a correspondingly high diffusion coefficient ratio in the macropore diffusion and transition pore diffusion stages (Fig. 6(a)). However, the corresponding relation is not obvious in the micropore diffusion stage owing to the low micropore content. A comparison diagram of the diffusion coefficient ratio and micropore volume is plotted separately in Fig. 6(b). The image suggests little correlation between the diffusion coefficient ratio and pore volume fraction in the micropore diffusion stage. Figure 6(c) shows a good correlation between the diffusion coefficient ratio and the specific surface fraction, and only SY 15# has a large outlier in the transition diffusion stage, indicating that the three diffusion processes with the multiporous diffusion model are controlled by the surface areas of the three pore scales in the coal reservoir. The increased surface area of coal provides more sorption sites, and more molecules would migrate at the critical point of adsorption-desorption equilibrium, resulting in an increase in methane diffusion

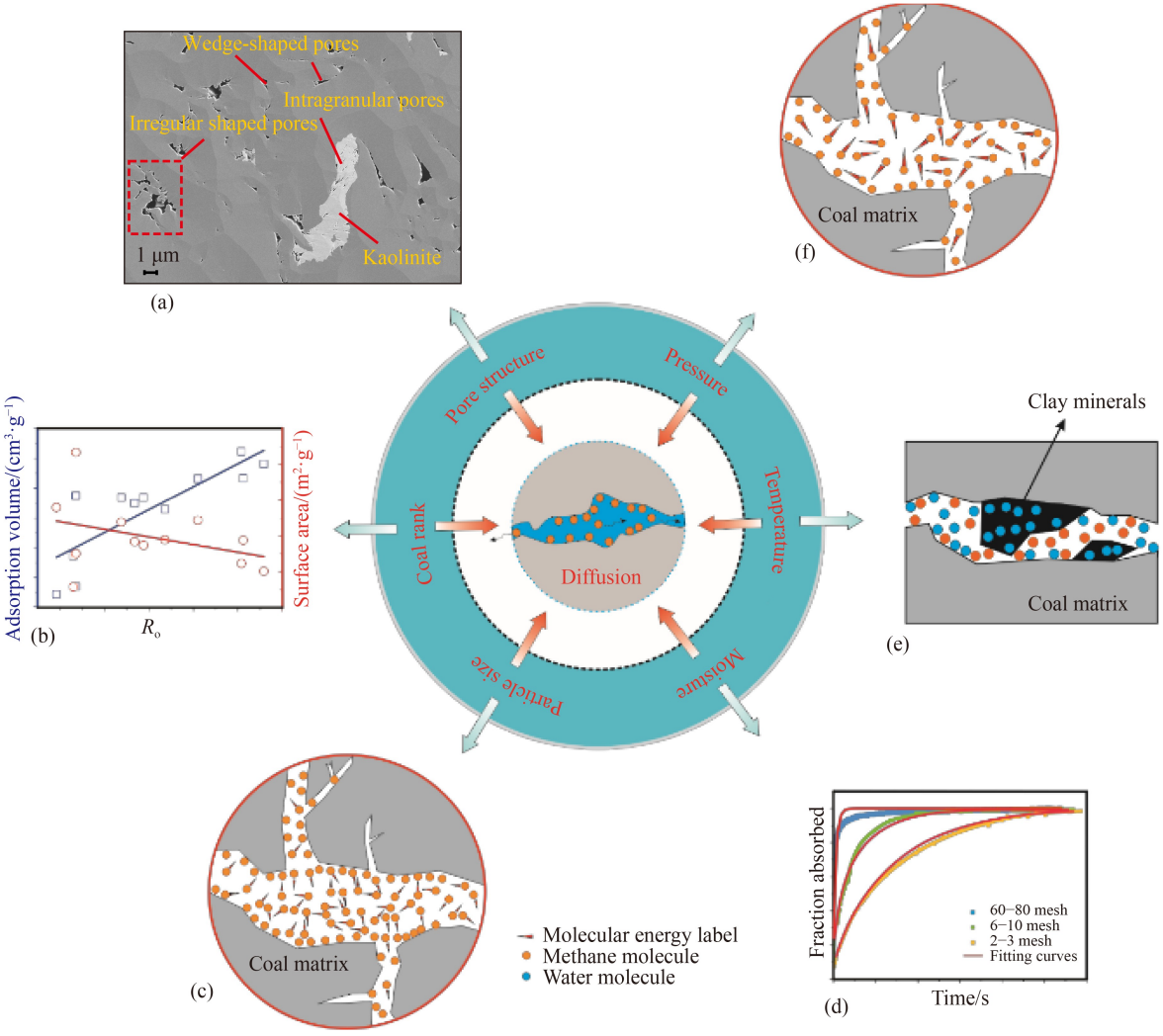

Fig. 5 Schematic of diffusion influencing factors (a) morphology of pore-fractures from FESEM images; (b) relationship between coal rank and adsorption capacity or pore surface area; (c) diffusivity in coals with different particle size; (d) clay minerals swelling when absorbing moisture; (e) molecular motion at high temperature; (f) molecular motion at high pressure.

Table 2 The integrated data of pore volume and pore surface area by MIP and low-temperature nitrogen analysis

Sample No.	Integrated pore volume distribution/(10^{-3} cm^3·g^{-1})				Integrated pore surface area distribution/(m^2·g^{-1})			
	<10 nm	10–10^2 nm	10^2–10^3 nm	>10^3 nm	<10 nm	10–10^2 nm	10^2–10^3 nm	>10^3 nm
LHJ 4#	0.308	1.112	29.484	7.186	0.373	0.163	0.001	0.016
FL 1#	0.158	0.667	1.406	11.032	0.086	0.025	0.105	0.826
HDG 6#	0.486	2.019	12.818	2.332	0.553	0.270	0.159	0.029
BD 2#	0.475	0.875	5.332	16.275	0.230	0.067	0.089	0.272
YT 5#	0.348	1.284	3.617	21.265	0.329	0.130	0.079	0.466
HJG 5#	0.202	0.567	2.741	9.274	0.286	0.070	0.035	0.119
WJY 8#	0.263	0.720	1.764	26.445	0.271	0.065	0.047	0.710
DQ 4#	0.285	0.481	11.813	1.597	0.323	0.045	0.143	0.019
SY 15#	0.321	1.181	2.048	16.692	0.343	0.126	0.033	0.270
XY 15#	0.046	0.487	0.934	10.992	0.099	0.129	0.031	0.361
DY 6#	0.241	0.745	8.069	0.632	0.279	0.083	0.094	0.007
GZ 15#	0.257	0.827	1.512	8.891	0.007	0.165	0.047	0.278

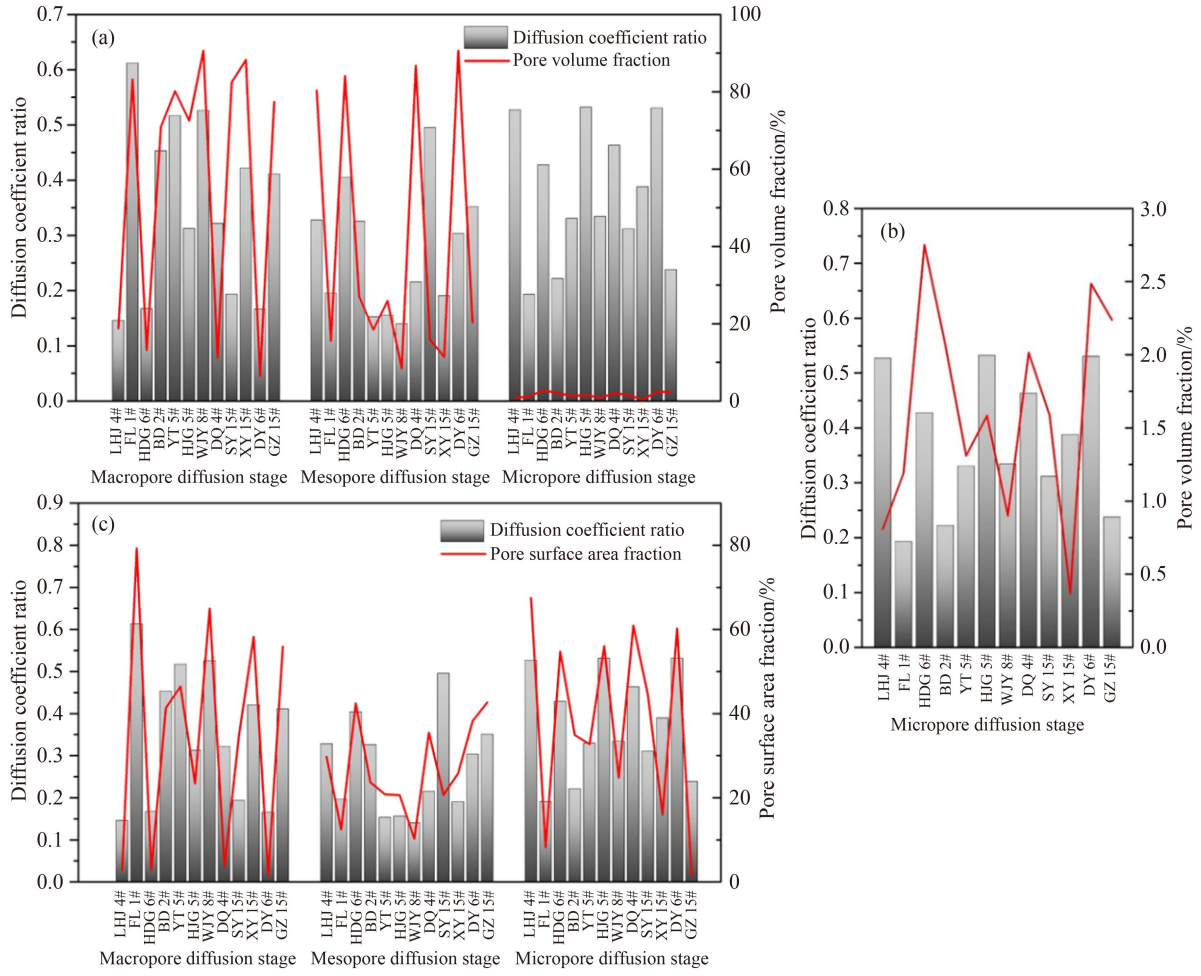

Fig. 6 (a) Composite graph of diffusion coefficient ratio and pore volume fraction of different diffusion stage; (b) redraw the micropore diffusion stage in (a); (c) composite graph of diffusion coefficient ratio and pore surface area fraction of different diffusion stage.

(Zhao et al., 2016). Thus, the larger the pore surface area, the more significant the surface diffusion.

4.1.2 Coal rank

Putting the diffusivities into a line chart versus $R_{o,m}$, the figures show that the broken lines of macropore diffusivity (M_{ae}), transitional diffusivity (M_{ee}), and micropore diffusivity(M_{ie}) present a "U" shape (Fig. 7(a)). Methane diffusivity is mainly related to the pore structure characteristics and adsorption capacity of coals of different ranks (Crosdale et al., 1998; Clarkson and Bustin, 1999; Liu et al., 2018b). The more developed the surface area or the higher the adsorption capacity, the greater the effective diffusion coefficient. The surface area of coal decreases with an increase in coal rank, whereas the adsorption capacity of coal increases with an increase in coal rank (Fig. 5(b)).

The adsorption capacity of coal is controlled by the pore structure and the maceral composition; the adsorption capacity increases as the total content of vitrinite and inertinite increases (Yao et al., 2008). In this study, the total content of vitrinite and inertinite increased with increasing coal rank (Table 1). The results showed that coal with a larger surface area had a smaller adsorption capacity when the influence of vitrinite and inertinite on the adsorption capacity was greater than that of the surface area. Therefore, the "U" shaped diffusion coefficient curve is the result of the combined action of specific surface and adsorption capacity.

4.1.3 Pressure

As shown in Fig. 7(b), the variation in the values of the three methane diffusion coefficients with pressure was bimodal. There is a negative correlation between the diffusion coefficient and pressure at low pressures, whereas the curve flattens out at high pressures. This conclusion is in contrast to the study of Si et al. (2021), in which the diffusion experiment was conducted in a water-saturated environment. The pressure caused the seepage of gas in the residual pores, leading to a larger contact area between the gas and water-saturated pores and more diffusion paths.

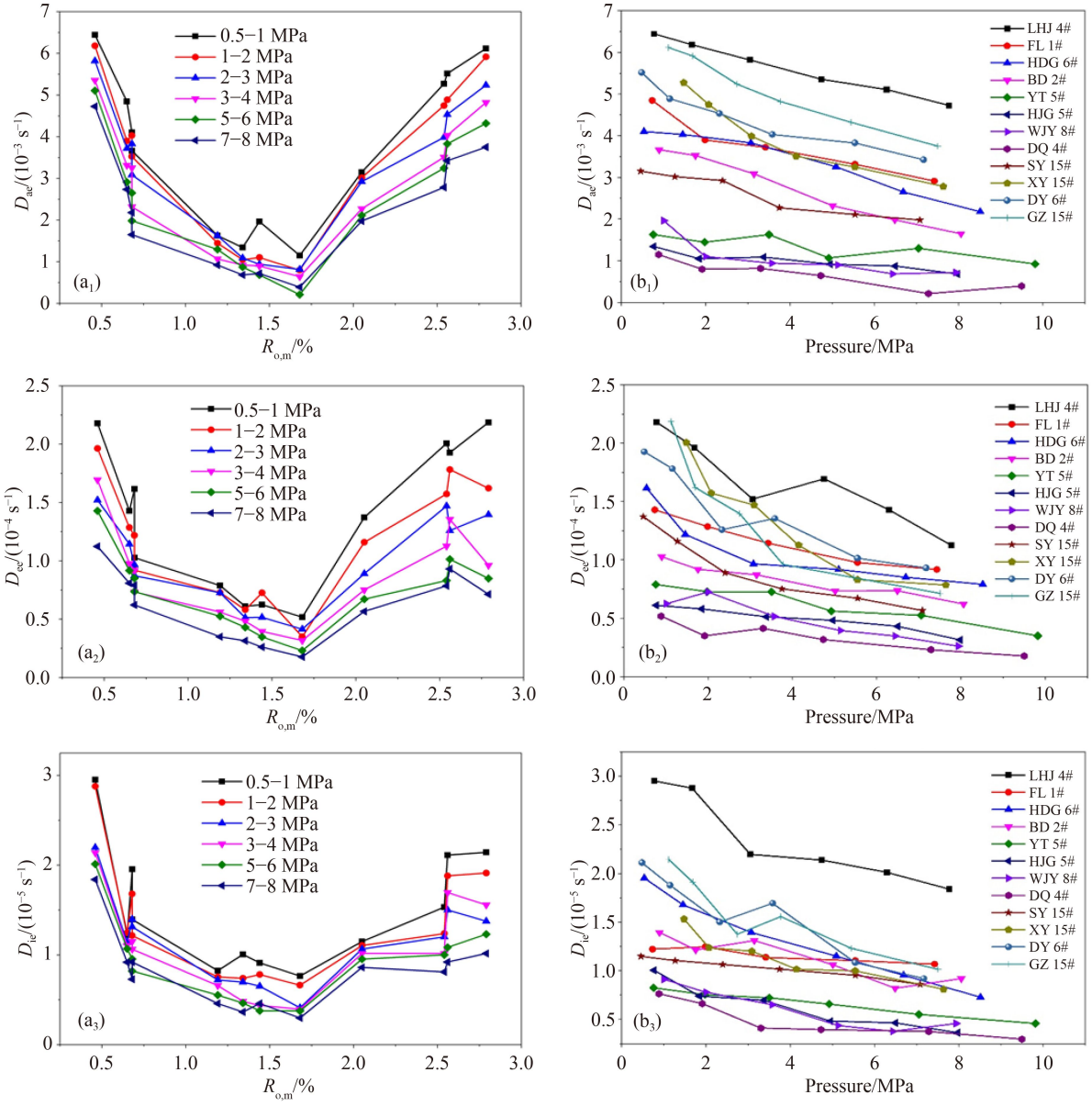

Fig. 7 (a) Methane diffusivities of different rank coal samples using multiporous model; (b) methane diffusivities with pressure using multiporous model. Notes: D_{ae}: the macropore effective diffusion coefficient; D_{ee}: the transition pore and mesopore effective diffusion coefficient; D_{ie}: the micropore effective diffusion coefficient.

Diffusive flow in a coal reservoir can be influenced by three distinct mechanisms: Fickian, Knudson, and surface diffusion (Rigby, 2005; Pan et al., 2010; Zeng et al., 2019). Fickian diffusion involves intermolecular collisions between gas molecules and tends to dominate large pores, which corresponds to the fast macropore diffusion stage. Knudsen diffusion dominates when the mean free path of the gas molecule is greater than the pore size, and collisions occur between the gas molecules and the pore walls, which corresponds to a much slower micropore diffusion stage. The intermediate rate transition diffusion stage is influenced by the combination of Fickian and Knudsen diffusion. Surface diffusion occurs during the entire diffusion process, and it is important when the molecules are strongly adsorbed and move along the surface of the pore. Surface diffusion is a function of the amount adsorbed, which increases as the quantity of adsorbed dye increases (Medveď and Černý, 2011). The density of gas increases with increasing pressure, resulting in a decrease in the intermolecular distance and the mean free path of methane molecules (Fig. 5(c)), which causes some methane molecules in Fickian diffusion to change into Knudsen diffusion. At low pressures, more methane is adsorbed on the surface of the coal matrix with an increase in pressure, and then more surface diffusion occurs, resulting in a rapid decrease in the diffusion coefficient. At high pressures, the adsorption capacity increases slowly to the adsorption-

desorption equilibrium, resulting in a slow increase in surface diffusion. Thus, the methane diffusion coefficient decreases significantly at low pressures, resulting in faster gas desorption in low-pressure ranges. This finding can have a significant impact on the projection of methane production from coal at low pressure.

4.1.4 Particle size

When the particle size changes from 60 to 80 mesh to 2–3 mesh, the macropore diffusivity, transition diffusivity, and micropore diffusivity decreases by approximately 60%, 63%, and 57% on average, respectively, which is shown in Fig. 8(a). Figure 5(d) shows the fraction of gas desorbed with a time of FL 1# samples with three particle sizes from 0.51 to 0.74 MPa. The results show that more time is needed to reach the diffusion equilibrium with the increase of coal particle size.

According to Groen et al. (2003), a smaller sample particle size does not significantly increase the specific surface area but only slightly increases the external surface area of coal particles, and the external surface area is negligible relative to the pore specific surface area. Small coal particles correspond to a simple pore topology and low diffusion resistance (Sander et al., 2020), and the increase in particle size results in a longer effective diffusion path and a higher tortuosity factor affecting the diffusion influx in porous media. Thus, a coal sample with a larger particle size has a smaller effective diffusion coefficient.

4.1.5 Moisture content

The macropore diffusivity, transition diffusivity, and micropore diffusivity decreased by 93%, 87%, and 83%, respectively, with increased moisture content, as shown in Fig. 8(b). Coal mainly consists of aromatic macromolecular structures and side chains composed of small molecules. The small molecules contain hydrocarbon groups (–CH_3 and –CH_2) and polar hydrophilic groups (–COOH, –CO, –OCH_3, and –OH), and the former easily adsorbs hydrocarbons, whereas the latter easily adsorbs H_2O, O_2, N_2, CO_2, and other gases (Liu et al., 2019b). There is a strong chemical binding force between the polar functional groups and H_2O molecules, and moisture adsorbs more easily to the pore surface than methane

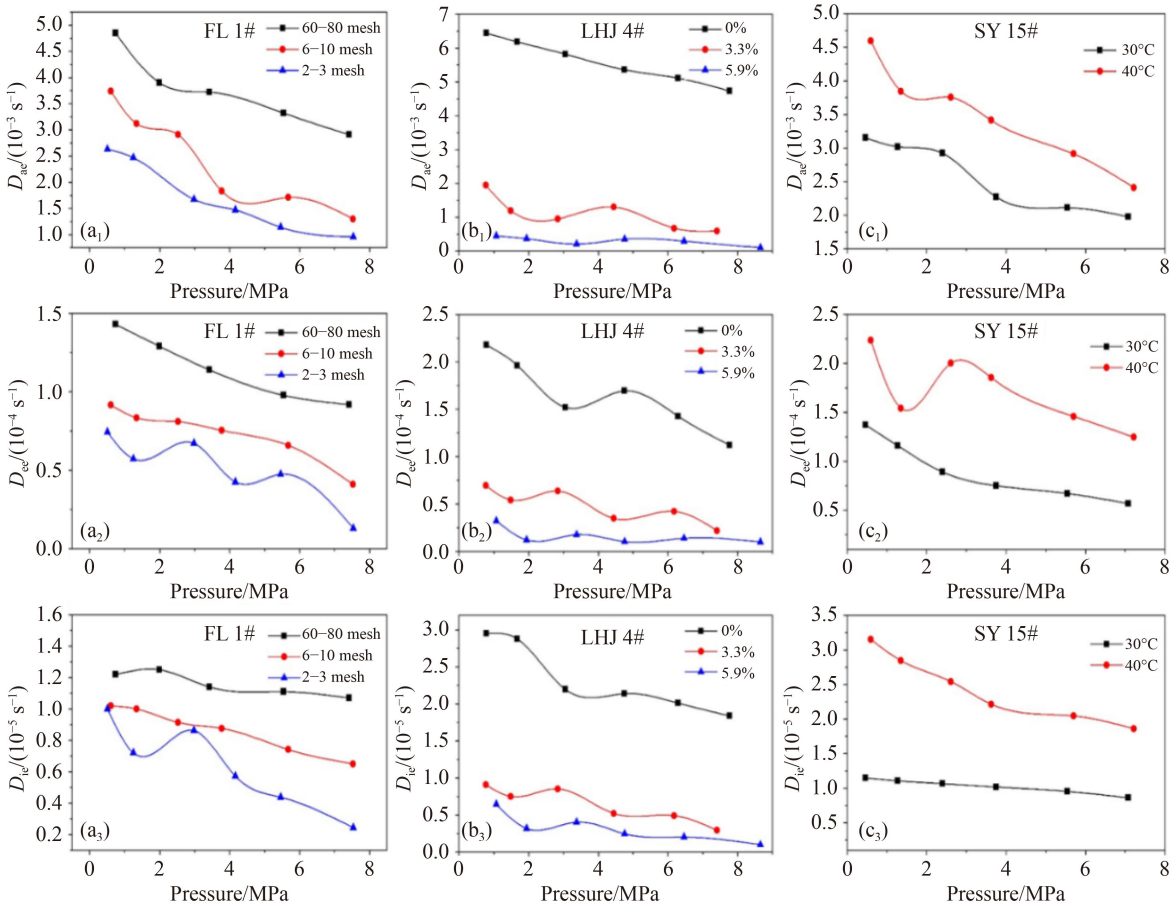

Fig. 8 (a) Methane diffusivities with particle size; (b) methane diffusivities with moisture content; (c) methane diffusivities with temperature using multiporous model. Notes: D_{ae}: macropore effective diffusion coefficient; D_{ee}: transition pore and mesopore effective diffusion coefficients; D_{ie}: micropore effective diffusion coefficient.

molecules. Water clusters may occur and occupy the free pore space, which is unfavorable for gas adsorption and diffusion. In addition, clay minerals such as illite and montmorillonite may swell when absorbing moisture, which possibly reduces the original pore volume and narrows the pore throats (Fig. 5(e)).

4.1.6 Temperature

Figure 8(c) shows the methane diffusivities obtained from the multiporous model at different SY 15 # temperatures. The macropore, transition, and micropore diffusivities increased by 26%, 47%, and 55%, respectively, when the experimental temperature was changed from 30°C to 40°C (Supplementary material). The effects of temperature on methane diffusivities in the coal matrix can be interpreted using thermodynamic theories and molecular dynamics. Because gas diffusion is an endothermic process, the increasing temperature is favorable for the adsorption-diffusion equilibrium state to move toward the diffusion direction. Second, high temperatures increase the velocity and weaken the adsorbability of gas molecules (Si et al., 2021), which is conducive to improving the diffusion rate of methane (Fig. 5(f)). In addition, increasing the temperature causes the coal matrix to expand outward, opening up the pores and increasing the methane diffusion channel.

4.2 Comprehensive evaluation of methane diffusion controlling factors

A study on the influencing factors of methane diffusion shows that the methane diffusion coefficient first decreases and then increases with coal rank, which is due to the combined action of the specific surface and adsorption capacity. The presence of water significantly reduces the diffusion capacity of CBM as a result of water molecules occupying the pore space in the coal matrix and clay mineral swelling when absorbing moisture. The increase in particle size increases the diffusion path, and thus, a longer time is required to reach desorption equilibrium. Elevated temperatures would facilitate diffusion capacity because the rms velocity and mean free path of gas molecules would increase at higher temperatures. High pressure impedes methane diffusion because of the greater resistance generated by collisions between molecules. These factors are not physical quantities of the same dimension (Fig. 5); therefore, it is difficult to find the most effective factor for methane diffusion because each factor was studied separately using the control variable method.

In this study, gray relational analysis (GRA) was employed to analyze and verify the influence of coal rank, pore structure, particle size, moisture content, temperature, and pressure on methane diffusion in a coal reservoir. Grey systems theory has been developed as an emerging scientific discipline, with its theoretical structure consisting of systems analysis, evaluation, modeling, prediction, decision making, control, and techniques of optimization (Liu et al., 2012). Through gray relational analysis, the data were normalized and made dimensionless, and all factors affecting diffusion were unified into the same parameter, gray relation grade (r_i). Thus, a unified and intuitive comparison standard is obtained. This method has been applied to coal geology by many scholars, and research has proven the applicability of GRA in the analysis of influencing factors (Zhang et al., 2016; Xu et al., 2021).

The reference sequence consisting of methane diffusion coefficients is denoted by $\{X_0^{(0)}(i)\},(i = 1,2,\ldots,n)$. The comparison sequence, which is denoted by $\{X_t^{(0)}(i)\}(t = 1,2,\ldots,m),(i = 1,2,\ldots,n)$ is composed of several influencing factors, including coal rank, pore volume, pore surface area, particle size, moisture content, temperature, and pressure, as listed in Table 3.

After preprocessing, the data in the sequence can be substituted into Eq. Seven to produce the gray relational coefficient, where $\rho = 0.5$, m is the number of influencing factors ($m = 7$), and n is the number of experimental data ($n = 22$). The gray relational grade (r_i) indicates the degree of influence that the comparability sequence can exert over the reference sequence. The values of gray relational grade for each factor affecting methane diffusion are shown in Fig. 9, the importance of these factors on methane diffusion was identified in order from the most important to the least: particle size > moisture > surface area > pore volume > pressure > coal rank > temperature in all of three diffusion stages. The weight of the particle size (20%) is much greater than that of the other factors; therefore, the particle size is the most crucial factor for methane diffusion in coal reservoirs. The effect of the particle size on diffusion is due to changes in the diffusion path and tortuosity. Therefore, the most effective enhancement scheme for methane diffusion is to shorten the diffusion distance, according to the analysis results of the main factors controlling methane diffusion.

5 Conclusions

In this work, the multiscale micro-nano pore system in various rank coals was quantitatively characterized, and isothermal adsorption-diffusion experiments using the volumetric method were conducted to explore the influencing factors of methane diffusion in micro-nano coal pores based on different diffusion models. The following conclusions were drawn.

1) The development characteristics of seepage pores (>100 nm) and adsorption pores (<100 nm) in different coal ranks were quantitatively characterized. The results showed that the pore structure of the coals exhibited a multimodal pore size/volume distribution. There are irregular oval pores (accounting for approximately 20%),

Table 3 Methane diffusion coefficients and test data of each influencing factor

Sample No.	Methane diffusion coefficients			$R_{o,m}$/%	S_{BET}/($m^2 \cdot g^{-1}$)	V_{BJH}/($\times 10^{-3} cm^3 \cdot g^{-1}$)	P/MPa	A/mm	M/%	T/°C
	D_{ae}/s^{-1}	D_{ee}/s^{-1}	D_{ie}/s^{-1}							
LHJ 4#-01	6.44E-03	2.18E-04	2.95E-05	0.46	0.559	2.282	0.78	0.215	0	30
LHJ 4#-02	1.20E-03	5.43E-05	7.51E-06	0.46	0.559	2.282	1.48	0.215	3.3	30
LHJ 4#-03	3.53E-04	1.04E-05	2.47E-06	0.46	0.559	2.282	4.76	0.215	5.9	30
FL 1#-01	3.90E-03	1.29E-04	1.25E-05	0.65	0.116	0.467	1.99	0.215	0	30
FL 1#-02	2.91E-03	8.10E-05	9.15E-06	0.65	0.116	0.467	2.52	2.525	0	30
FL 1#-03	1.47E-03	4.26E-05	5.73E-06	0.65	0.116	0.467	4.16	7.35	0	30
HDG 6#	4.03E-03	1.22E-04	1.68E-05	0.68	0.867	4.207	1.46	0.215	0	30
BD 2#-01	3.66E-03	1.03E-04	1.40E-05	0.68	0.301	1.701	0.9	0.215	0	30
BD 2#-02	5.14E-03	1.93E-04	3.21E-05	0.68	0.301	1.701	0.83	0.215	0	40
YT 5#	1.63E-03	7.27E-05	7.22E-06	1.19	0.477	2.546	3.5	0.215	0	30
HJG 5#	1.09E-03	5.14E-05	6.97E-06	1.34	0.367	1.232	3.38	0.215	0	30
WJY 8#	9.41E-04	5.16E-05	6.53E-06	1.44	0.347	1.574	3.57	0.215	0	30
DQ 4#	2.12E-04	2.31E-05	3.76E-06	1.68	0.378	1.279	7.28	0.215	0	30
SY 15#-01	3.15E-03	1.37E-04	1.15E-05	2.05	0.487	2.339	0.46	0.215	0	30
SY 15#-02	3.75E-03	2.00E-04	2.54E-05	2.05	0.487	2.339	2.61	0.215	0	40
XY 15#	3.25E-03	8.32E-05	1.00E-05	2.54	0.246	0.867	5.54	0.215	0	30
DY 6#	3.83E-03	1.01E-04	1.09E-05	2.56	0.375	1.595	5.54	0.215	0	30
GZ 15#-01	3.75E-03	7.14E-05	1.02E-05	2.79	0.202	1.662	7.5	0.215	0	30
GZ 15#-02	2.94E-03	8.18E-05	1.06E-05	2.79	0.202	1.662	1.35	2.525	0	30
GZ 15#-03	1.59E-03	4.23E-05	4.54E-06	2.79	0.202	1.662	3.74	7.35	0	30
GZ 15#-04	1.26E-03	4.29E-05	5.12E-06	2.79	0.202	1.662	2.6	0.215	2.3	30
GZ 15#-05	1.24E-04	1.06E-05	2.00E-06	2.79	0.202	1.662	7.14	0.215	4.1	30

Notes: D_{ae}- Macropore effective coefficient; D_{ee}- Transition pore and mesopore effective coefficient; D_{ie}- Micropore effective coefficient; S_{BET} - BET surface area; V_{BJH} - BJH total pore volume; P - Pressure; A - Particle size; M - Moisture content; T- Temperature.

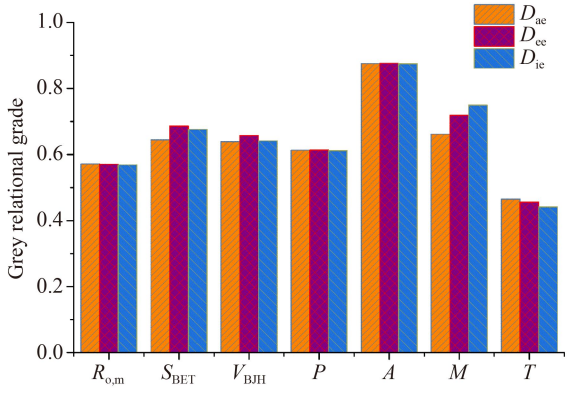

Fig. 9 The gray relational grade for seven comparability sequences with three diffusion stage.

Notes: D_{ae}: macropore effective coefficient; D_{ee}: transition pore and mesopore effective coefficient; D_{ie}: micropore effective coefficient; S_{BET}: BET surface area; V_{BJH}: BJH total pore volume; P: pressure; A: particle size; M: moisture content; T: temperature.

wedge-shaped and slit-like pores (accounting for approximately 50%), and short linear-like pores (accounting for approximately 20%) in low-medium rank bituminous coal, whereas multitudinous metamorphic pores develop in high-rank bituminous coal and anthracite, accounting for approximately 70%.

2) Methane diffusion in the multi-scale pores of coal reservoirs exhibits the characteristics of early fast diffusion, transitional diffusion in the medium term, and slow diffusion in the later period. The surface area proportions of micropores, transition pores, mesopores, and macropores in the coal reservoir correspond well with the diffusion stages, indicating that the multiporous diffusion model is more suitable for describing the methane adsorption-diffusion process.

3) The influencing factors and mechanisms of methane diffusion in coal were systematically analyzed. The results show that the diffusion coefficient of methane first decreases and then increases with an increase in the coal rank. The presence of water significantly reduces the diffusion capacity of CBM, and the increase in particle size reduces the diffusion rate by increasing the diffusion path. An elevated temperature would facilitate diffusion capacity, whereas a high pressure is supposed to impede methane diffusion.

4) Grey relational analysis was employed to analyze and verify the importance of the factors affecting methane diffusion. The impact ranking of factors, as an order from the most important to the least: particle size > moisture > surface area > pore volume > pressure > coal rank > temperature in all of three diffusion stages. The particle size (weight of 20%) is the most effective factor for methane diffusion in coal reservoirs.

Although the impact ranking of the factors affecting methane diffusion is estimated using GRA, the model does not explain how these factors interact in nature. Thus, other analysis models need to be established to analyze the influence mechanism between each factor in follow-up studies.

Supplementary material is available in the online version of this article at http://dx.doi.org/10.1007/s11707-022-0992-3 and is accessible for authorized users.

Acknowledgments This research was funded by the National Natural Science Foundation of China (Grant Nos. 41922016, 41830427, and 41772160), the Fundamental Research Funds for the Central Universities (No. 2652019264).

References

Bai L H, Liu B, Du Y J, Wang B Y, Tian S S, Wang L, Xue Z Q (2021). Distribution characteristics and oil mobility thresholds in lacustrine shale reservoir: insights from N_2 adsorption experiments on samples prior to and following hydrocarbon extraction. Petrol Sci, 19(2): 486–497

Busch A, Gensterblum Y, Krooss B M, Littke R (2004). Methane and carbon dioxide adsorption-diffusion experiments on coal: upscaling and modeling. Int J Coal Geol, 60(2–4): 151–168

Cai Y D, Li Q, Liu D M, Zhou Y F, Lv D (2018). Insights into matrix compressibility of coals by mercury intrusion porosimetry and N_2 adsorption. Int J Coal Geol, 200: 199–212

Cai Y D, Pan Z J, Liu D M, Zheng G Q, Tang S H, Connell L D, Yao Y B, Zhou Y F (2014). Effects of pressure and temperature on gas diffusion and flow for primary and enhanced coalbed methane recovery. Energy Explor Exploit, 32(4): 601–619

Charrière D, Pokryszka Z, Behra P (2010). Effect of pressure and temperature on diffusion of CO_2 and CH_4 into coal from the Lorraine Basin (France). Int J Coal Geol, 81(4): 373–380

Chen S B, Li X Y, Chen S, Wang Y, Gong Z, Zhang Y K (2021). A new application of atomic force microscopy in the characterization of pore structure and pore contribution in shale gas reservoirs. J Nat Gas Sci Eng, 88: 103802

Clarkson C R, Bustin R M (1999). The effect of pore structure and gas pressure upon the transport properties of coal: a laboratory and modeling study. 2. Adsorption rate modeling. Fuel, 78(11): 1345–1362

Crank J (1956). The Mathematics of Diffusion. Oxford: The Clarendon Press

Crosdale P J, Beamish B B, Valix M (1998). Coalbed methane sorption related to coal composition. Int J Coal Geol, 35(1–4): 147–158

Desbois G, Urai J L, Kukla P A, Konstanty J, Baerle C (2011). High-resolution 3D fabric and porosity model in a tight gas sandstone reservoir: a new approach to investigate microstructures from mm- to nm-scale combining argon beam cross-sectioning and SEM imaging. J Petrol Sci Eng, 78(2): 243–257

Fang X L, Cai Y D, Liu D M, Zhou Y F (2018). A mercury intrusion porosimetry method for methane diffusivity and permeability evaluation in coals: a Comparative analysis. Appl Sci (Basel), 8(6): 860

Groen J C, Peffer L A A, Pérez-Ramírez J (2003). Pore size determination in modified micro- and mesoporous materials. Pitfalls and limitations in gas adsorption data analysis. Microporous Mesoporous Mater, 60(1–3): 1–17

Guo H J, Yuan L, Cheng Y P, Wang K, Xu C, Zhou A, Zang J, Liu J J (2018). Effect of moisture on the desorption and unsteady-state diffusion properties of gas in low-rank coal. J Nat Gas Sci Eng, 57: 45–51

Bytee K (2004). Coalbed-methane reservoir simulation: an evolving science. J Pet Technol, 56(4): 61–63

Hu H X, Li X C, Fang Z M, Wei N, Li Q S (2010). Small-molecule gas sorption and diffusion in coal: molecular simulation. Energy, 35(7): 2939–2944

Jia T, Liu C, Wei G, Yan J, Zhang Q, Niu L, Liu X, Zhang M, Ju Y, Zhang Y (2021). Micro-nanostructure of coal and adsorption-diffusion characteristics of methane. J Nanosci Nanotechnol, 21(1): 422–430

Karacan C Ö, Okandan E (2001). Adsorption and gas transport in coal microstructure: investigation and evaluation by quantitative X-ray CT imaging. Fuel, 80(4): 509–520

Li Z T, Liu D M, Cai Y D, Shi Y L (2016). Investigation of methane diffusion in low-rank coals by a multiporous diffusion model. J Nat Gas Sci Eng, 33: 97–107

Liu J, Qin Y P, Zhang S, He C (2019a). Numerical solution for borehole methane flow in coal seam based on a new dual-porosity model. J Nat Gas Sci Eng, 68: 102916

Liu P, Qin Y P, Liu S M, Hao Y J (2018b). Non-linear gas desorption and transport behavior in coal matrix: experiments and numerical modeling. Fuel, 214: 1–13

Liu S F, Forrest J, Yang Y J (2012). A brief introduction to grey systems theory. Grey Syst, 2(2): 89–104

Liu X F, Song D Z, He X Q, Nie B S, Wang L K (2019b). Insight into the macromolecular structural differences between hard coal and deformed soft coal. Fuel, 245: 188–197

Liu Z S, Liu D M, Cai Y D, Pan Z J (2018a). The impacts of flow velocity on permeability and porosity of coals by core flooding and nuclear magnetic resonance: implications for coalbed methane production. J Petrol Sci Eng, 171: 938–950

Lu X, Armstrong R T, Mostaghimi P (2020). Analysis of gas diffusivity in coal using micro-computed tomography. Fuel, 261: 116384

Medveď I, Černý R (2011).Surface diffusion in porous media: a critical review. Microporous Mesoporous Mater. 142: 405–422

Meng Y, Li Z P (2016). Experimental study on diffusion property of methane gas in coal and its influencing factors. Fuel, 185: 219–228

Moore T A (2012). Coalbed methane: a review. Int J Coal Geol,

101(1): 36–81

Pan Z J, Connell L D, Camilleri M, Connelly L (2010). Effects of matrix moisture on gas diffusion and flow in coal. Fuel, 89(11): 3207–3217

Pillalamarry M, Harpalani S, Liu S M (2011). Gas diffusion behavior of coal and its impact on production from coalbed methane reservoirs. Int J Coal Geol, 86(4): 342–348

Quan F K, Wei C T, Zhang J J, Feng S L, Hao S Q, Lu G W, Hu Y B (2020). Study on desorption and diffusion dynamics of coal reservoir through step-by-step depressurization simulation——an experimental simulation study based on LF-NMR technology. J Nat Gas Sci Eng, 75: 103149

Rigby S P (2005). Predicting surface diffusivities of molecules from equilibrium adsorption isotherms. Colloids Surf A Physicochem Eng Asp, 262(1–3): 139–149

Ruckenstein E, Vaidyanathan A S, Youngquist G R (1971). Sorption by solids with bidisperse pore structures. Chem Eng Sci, 26(9): 1305–1318

Salmachi A, Bonyadi M R, Sayyafzadeh M, Haghighi M (2014). Identification of potential locations for well placement in developed coalbed methane reservoirs. Int J Coal Geol, 131: 250–262

Sander R, Connell L D, Camilleri M, Pan Z J (2020). CH_4, CO_2, N_2 diffusion in Bowen Basin (Australia) coal: relationship between sorption kinetics of coal core and crushed coal particles. J Nat Gas Sci Eng, 81: 103468

Si L L, Zhang H T, Wei J P, Li B, Han H K (2021). Modeling and experiment for effective diffusion coefficient of gas in water-saturated coal. Fuel, 284: 118887

Smith D M, Williams F L (1984). Diffusional effects in the recovery of methane from coalbeds. Soc Pet Eng J, 24(5): 529–535

Staib G, Sakurovs R, Gray E A (2013). A pressure and concentration dependence of CO_2 diffusion in two Australian bituminous coals. Int J Coal Geol, 116–117: 106–116

Tosun N (2006). Determination of optimum parameters for multi-performance characteristics in drilling by using grey relational analysis. Int J Adv Manuf Technol, 28(5–6): 450–455

Wang X L, Zhang D M, Su E L, Jiang Z G, Wang C Y, Chu Y P, Ye C (2020). Pore structure and diffusion characteristics of intact and tectonic coals: implications for selection of CO_2 geological sequestration site. J Nat Gas Sci Eng, 81: 103388

Warren J E, Root P J (1963). The behavior of naturally fractured reservoirs. Soc Pet Eng J, 3: 245–255

Xu H, Tang D Z, Zhao J L, Li S, Tao S (2015). A new laboratory method for accurate measurement of the methane diffusion coefficient and its influencing factors in the coal matrix. Fuel, 158: 239–247

Xu S P, Hu E F, Li X C, Xu Y (2021). Quantitative analysis of pore structure and its impact on methane adsorption capacity of coal. Nat Resour Res, 30(1): 605–620

Yang R, Ma T R, Xu H, Liu W Q, Hu Y, Sang S (2019). A model of fully coupled two-phase flow and coal deformation under dynamic diffusion for coalbed methane extraction. J Nat Gas Sci Eng, 72: 103010

Yao Y B, Liu D M, Tang D Z, Tang S H, Huang W H (2008). Fractal characterization of adsorption-pores of coals from north China: an investigation on CH_4 adsorption capacity of coals. Int J Coal Geol, 73(1): 27–42

Zeng F H, Peng F, Guo J C, Wang D Y, Zhang S R, Zhang P, Zhang B (2019). Gas transport study in the confined microfractures of coal reservoirs. J Nat Gas Sci Eng, 68: 102920

Zhang H L, Wang J, Zhang H Y (2016). Investigation of the main factors during shale-gas production using grey relational analysis. Open Petrol Eng J, 9(1): 207–215

Zhang H (2001). Genetical type of proes in coal reservoir and its research significance. J China Coal Soc, 26: 40–44

Zhang K Z, Cheng Y P, Wang L, Dong J, Hao C M, Jiang J Y (2020). Pore morphology characterization and its effect on methane desorption in water-containing coal: an exploratory study on the mechanism of gas migration in water-injected coal seam. J Nat Gas Sci Eng, 75: 103152

Zhang S H, Tang S H, Tang D Z, Pan Z J, Yang F (2010). The characteristics of coal reservoir pores and coal facies in Liulin District, Hedong Coal Field of China. Int J Coal Geol, 81(2): 117–127

Zhao J L, Xu H, Tang D Z, Mathews J P, Li S, Tao S (2016). A comparative evaluation of coal specific surface area by CO_2 and N_2 adsorption and its influence on CH_4 adsorption capacity at different pore sizes. Fuel, 183: 420–431

Zhao Y X, Liu T, Danesh N N, Sun Y F, Liu S M, Wang Y (2020). Quantification of pore modification in coals due to pulverization using synchrotron small angle X-ray scattering. J Nat Gas Sci Eng, 84: 103669

Zheng S J, Yao Y B, Liu D M, Cai Y D, Liu Y (2018). Characterizations of full-scale pore size distribution, porosity and permeability of coals: a novel methodology by nuclear magnetic resonance and fractal analysis theory. Int J Coal Geol, 196: 148–158